Nonlocal quartic interactions and universality classes in perovskite manganites

Rohit Singh,[1,*] Kishore Dutta,[2,†] and Malay K. Nandy[1,‡]
[1]*Department of Physics, Indian Institute of Technology Guwahati, Guwahati 781 039, India*
[2]*Department of Physics, Handique Girls' College, Guwahati 781 001, India*
(Received 7 December 2014; published 16 July 2015)

A modified Ginzburg-Landau model with a screened nonlocal interaction in the quartic term is treated via Wilson's renormalization-group scheme at one-loop order to explore the critical behavior of the paramagnetic-to-ferromagnetic phase transition in perovskite manganites. We find the Fisher exponent η to be $O(\epsilon)$ and the correlation exponent to be $\nu = \frac{1}{2} + O(\epsilon)$ through epsilon expansion in the parameter $\epsilon = d_c - d$, where d is the space dimension, $d_c = 4 + 2\sigma$ is the upper critical dimension, and σ is a parameter coming from the nonlocal interaction in the model Hamiltonian. The ensuing critical exponents in three dimensions for different values of σ compare well with various existing experimental estimates for perovskite manganites with various doping levels. This suggests that the nonlocal model Hamiltonian contains a wide variety of such universality classes.

DOI: 10.1103/PhysRevE.92.012123 PACS number(s): 05.70.Jk, 05.10.Cc, 75.40.Cx

I. INTRODUCTION

The analytical investigation of the critical behavior of the paramagnetic-to-ferromagnetic (PM-FM) phase transition near the critical point using Wilson's renormalization-group (RG) scheme [1,2] has been a topic of much interest among researchers for a long time [3–8]. Most of these investigations considered a short-range (SR) interaction in the quartic term in the Ginzburg-Landau model Hamiltonian, and they describe the universality classes that depend on the space dimension d and the number of components n of the order parameter. It was Fisher, Ma, and Nickel [9] who analytically investigated, via Wilson's RG scheme, the critical behavior of an n-component Ginzburg-Landau (GL) model in d space dimensions in the presence of a long-range (LR) interaction incorporated in the quadratic part of the Hamiltonian as $\int\int d^d x\, d^d y \frac{\Phi(\mathbf{x})\,\Phi(\mathbf{y})}{|\mathbf{x}-\mathbf{y}|^{d+\sigma'}}$. Their analysis identified different regimes characterized by the LR exponent σ'. The results for the critical exponents were obtained via an ϵ' expansion about the mean field (where $\epsilon' = 2\sigma' - d$).

Over the past couple of decades, the critical properties of PM-FM phase transitions in perovskite manganite compounds ($R_{1-x}A_x MnO_3$) have been explored by various experiments [10–23]. [R stands for trivalent rare-earth elements (e.g., La, Nd, or Pr) and A stands for divalent alkaline-earth elements (e.g., Ca, Ba, or Sr)]. Although an initial experimental investigation [11] suggested inconclusive results with regard to the universality class, a number of subsequent experimental studies on some perovskite manganite samples [13,18,19,21] showed that the critical exponents were close to those of the tricritical mean-field theory ($\beta = \frac{1}{4}$, $\gamma = 1$, and $\delta = 5$) [24]. However, there are other perovskite manganite compounds [11,14–17,23] for which the critical exponents deviate from those of the tricritical mean-field values.

In some of these experimental works [11,15,19], the estimates for critical exponents were compared with those of the existing theoretical models, namely the mean-field, three-dimensional (3D) Ising, and 3D Heisenberg models. However, these existing models were unable to reproduce the critical exponents over a range of experimental samples. In fact, the above experiments indicated the existence of a wide range of universality classes with different choices for R and/or A as well as different levels of doping, x. It was found that a change in the doping level x in the same compound led to different critical exponents [11–13,15,18]. For instance, different sets of critical exponents were obtained for $La_{1-x}Ca_xMnO_3$ when $x = 0.2$ [12] and $x = 0.4$ [13]. Similar behavior was noted for $La_{1-x}Sr_xMnO_3$ when $x = 0.3$ [11] and $x = 0.125$ [15]. This was also observed in Ref. [18] for a different compound, namely $Nd_{1-x}Sr_xMnO_3$ with $x = 0.33$ and 0.4.

As we noted in the outset, a model with a long-range interaction in the quadratic term of the GL Hamiltonian was suggested by Fisher, Ma, and Nickel [9]. Motivated by their model, the corresponding critical behaviors were further investigated in a number of theoretical [25–32] as well as numerical [33–38] studies. Most of these studies were devoted to the investigation of a crossover between the LR and SR regions, mainly concentrating on the resolution of a jump discontinuity of the critical exponent η at the crossover value $\sigma' = 2$ [26,28–31,33,35,36]. Sak [26] showed via RG calculations that the jump discontinuity is smoothed out and the crossover takes place at $\sigma' = 2 - \eta_{SR}$, where η_{SR} is the SR value of the exponent η. In an attempt to find a representative theory for the PM-FM phase transition in perovskite manganites, we verified whether this LR theory can capture the critical behavior predicted by experiments on perovskite manganites. Table I shows the upper and lower bounds of various critical exponents obtained via RG calculations of Fisher, Ma, and Nickel incorporating Sak's correction for the continuity between the LR and SR regimes [9,26]. For $d = 3$, the tricritical values $\beta = \frac{1}{4}$ and $\delta = 5$ lie outside the ranges shown in Table I. Further, for $d = 2$, these values cannot be generated for any value of σ'; the exponent γ turns out to be unexpectedly higher (compared to the tricritical value $\gamma = 1$) for a matching value of $\beta = 0.25$. Moreover, the experimental values for the critical exponents away from tricriticality for a range of perovskite manganite samples cannot be realized consistently with the same theoretical estimates. Numerical simulations based on the same LR model

*rohit.singh@iitg.ernet.in
†kdkishore77@gmail.com
‡mknandy@iitg.ernet.in

TABLE I. Allowed ranges for the critical exponents for different values of d and n between lower and upper bounds, $[\sigma'_{\rm min},\sigma'_{\rm max}]$, of the long-range exponent σ', as predicted by the RG calculations of Ref. [9] incorporating the correction due to Sak [26]. The rows with single entries correspond to the best possible values nearest to the tricritical values as predicted by the same RG theory. The experimental ranges for the critical exponents (with error bars) obtained for samples given in Table II are also displayed in the last row for comparison.

d	n	σ'	α	β	γ	δ
	1	[1.5,1.981]	[0.0,0.082]	[0.5,0.338]	[1.0,1.240]	[3.0,4.076]
3	2	[1.5,1.980]	[0.018, − 0.013]	[0.5,0.359]	[1.0,1.296]	[3.0,4.083]
	3	[1.5,1.979]	[0.003, − 0.092]	[0.5,0.375]	[1.0,1.341]	[3.0,4.084]
	1	[1.0,1.926]	[0.058, − 0.003]	[0.5,0.183]	[1.0,1.636]	[3.0,5.320]
2	2	[1.0,1.920]	[0.013, − 0.254]	[0.5,0.232]	[1.0,1.790]	[3.0,5.358]
	3	[1.0,1.917]	[0.0, − 0.462]	[0.5,0.272]	[1.0,1.917]	[3.0,5.367]
	1	1.646	0.012	0.251	1.485	4.812
2	2	1.830	−0.237	0.250	1.737	5.209
	3	1.917	−0.462	0.272	1.917	5.367
Exptl. Range				[0.23(2),0.404(1)]	[0.948(8),1.45]	[4.12(33),5.17(2)]

[36,39,40] were also focused on the crossover, particularly for $d = 2$, and a smooth interpolation was obtained between the SR and LR regimes. However, they found $\eta_{\rm SR} \approx 0.25$, which is much higher than that predicted by Sak [26], thus excluding the possibility of explaining the exponents near and away from tricriticality. Thus a wide range of exponents observed for perovskite manganites near as well as away from tricriticality remain unexplained. This necessitates an alternative theoretical model capable of capturing the wide range of critical behavior of perovskite manganites, including their (nearly) tricritical behavior.

A common feature of the above-mentioned analytical as well as numerical works was the incorporation of the long-range effect in the quadratic (Φ^2) term of the model Hamiltonian, which did not affect the quartic (Φ^4) interaction term. The original Φ^4 term in the Ginzburg-Landau functional is equivalent to a contact or short-range interaction of the order-parameter field $\Phi(\mathbf{x})$. However, as suggested by Ma [5], this term can be generalized to a nonlocal interaction term as $\int d^dx \int d^dx'\ \Phi^2(\mathbf{x})u(\mathbf{x}-\mathbf{x}')\Phi^2(\mathbf{x}')$, where $u(\mathbf{x}-\mathbf{x}')$ is a coupling function that *modifies* the interactions among the different modes in Fourier space. In this paper, we analytically treat this nonlocal model for an n-component order parameter $\Phi(\mathbf{x})$, expressed by the Hamiltonian

$$H[\Phi] = \int d^dx \left[\frac{c_0}{2}|\nabla\Phi(\mathbf{x})|^2 + \frac{r_0}{2}\Phi^2(\mathbf{x}) + \int d^dx'\Phi^2(\mathbf{x})u(\mathbf{x}-\mathbf{x}')\Phi^2(\mathbf{x}') \right], \quad (1)$$

where $\Phi^2 = \sum_{i=1}^n \phi_i^2$ and $|\nabla\Phi|^2 = \sum_{i=1}^n \nabla\phi_i \cdot \nabla\phi_i$, with a screened nonlocal interaction represented by the coupling function

$$u(\mathbf{k}) = \frac{\lambda_0}{[\mathbf{k}^2 + m^2]^\sigma} \quad (2)$$

in the Fourier space, where λ_0 is a coupling constant and m is a screening parameter.

It may be noted that a different kind of nonlocality in the Φ^4 term was found to originate in the case of an elastic isotropic system, as a consequence of LR strain interactions [41]. Tröster performed a numerical simulation on the compressible nonlocal Φ^4 model and found convincing evidence for a tricritical point [41]. We may thus expect that our above-mentioned nonlocal model given by Eqs. (1) and (2) may capture the tricritical property as well as the features near a tricritical point. It would be interesting to explore this model via an RG analysis and compare the ensuing critical exponents with those of the experimental perovskite manganites samples that exhibit critical behavior near and away from tricriticality.

In this paper, we carry out a Wilson-type RG scheme at one-loop order and calculate the critical exponents in the leading order of $\epsilon = d_c - d$, where the critical dimension turns out to be $d_c = 4 + 2\sigma$. We find that the critical exponents for various values of σ for $n = 3$ in three dimensions with small screening are in good agreement with experimental estimates for a wide range of perovskite manganites as displayed in Table II. Thus, it is evident that the model Hamiltonian with such nonlocal mode-coupling interactions [Eqs. (1) and (2)] contains a wide range of universality classes including the tricriticality in perovskite manganites.

The paper is organized as follows. In Sec. II, we carry out the renormalization-group scheme with the nonlocal model Hamiltonian at one-loop order. The critical exponents are calculated in the leading order of ϵ in Sec. III, where a comparison of our analytical results with experimental findings is also given. Finally, Sec. IV presents discussions and the conclusions of the work.

II. RENORMALIZATION-GROUP SCHEME

Our starting point is the modified Ginzburg-Landau Hamiltonian given by Eq. (1), where we incorporated the effect of long-range interactions in the quartic term. To carry out the Wilsonian momentum shell RG scheme [1,4,8], we Fourier-transform the order parameter field $\Phi(\mathbf{x})$ in d dimensions as

$$\phi_i(\mathbf{x}) = \int \frac{d^dk}{(2\pi)^d}\,\phi_i(\mathbf{k})\,e^{i\mathbf{k}\cdot\mathbf{x}} \quad (3)$$

TABLE II. Comparison of the critical exponents β, γ, and δ following from Eqs. (30), (31), and (32) for $n = d = 3$ and $w = 0.001$ with experimental estimates obtained for various perovskite manganite compounds.

σ	Experimental sample	Ref.	β	γ	δ
−0.499			0.250	1.000	4.999
	$La_{0.6}Ca_{0.4}MnO_3$ (PC[a])	[13]	0.25 ± 0.03	1.03 ± 0.05	5.0 ± 0.8
	$La_{0.6}Ca_{0.4}MnO_3$ (PC)	[21]	0.248	0.995	4.896
	$Nd_{0.67}Sr_{0.33}MnO_3$ (PC)	[18]	0.23 ± 0.02	1.05 ± 0.03	5.13 ± 0.04
	$La_{0.1}Nd_{0.6}Sr_{0.3}MnO_3$ (PC)	[19]	0.248 ± 0.006	1.066 ± 0.002	
−0.463			0.257	1.015	4.936
	$La_{0.1}Nd_{0.6}Sr_{0.3}MnO_3$ (PC)	[19]	0.257 ± 0.005	1.12 ± 0.03	5.17 ± 0.02
−0.325			0.288	1.080	4.633
	$La_{0.5}Ca_{0.3}Ag_{0.2}MnO_3$ (PC)	[22]	0.288 ± 0.002	0.948 ± 0.008	4.90 ± 0.02
−0.300			0.295	1.094	4.577
	$La_{0.7}Sr_{0.3}MnO_3$ (SC[b])	[10]	0.295 ± 0.002		
−0.243			0.311	1.129	4.454
	$La_{0.5}Ca_{0.4}Ag_{0.1}MnO_3$ (PC)	[22]	0.311 ± 0.003	1.146 ± 0.006	4.83 ± 0.01
−0.203			0.324	1.157	4.371
	$La_{0.67}Sr_{0.16}Ca_{0.17}MnO_3$ (PC)	[23]	0.324 ± 0.005	1.176 ± 0.03	4.415 ± 0.02
−0.193			0.328	1.164	4.351
	$La_{0.8}Ca_{0.2}MnO_3$	[20]	0.328	1.193	4.826
−0.150			0.344	1.199	4.268
	$Pr_{0.77}Pb_{0.23}MnO_3$ (SC)	[17]	0.344 ± 0.001	1.352 ± 0.006	4.69 ± 0.02
−0.115			0.360	1.231	4.203
	$La_{0.8}Ca_{0.2}MnO_3$ (SC)	[12]	0.36	1.45	5.03
−0.094			0.370	1.251	4.164
	$La_{0.7}Sr_{0.3}MnO_3$ (SC)	[11]	0.37 ± 0.04	1.22 ± 0.03	4.25 ± 0.2
−0.095			0.370	1.250	4.166
	$La_{0.875}Sr_{0.125}MnO_3$ (SC)	[15]	0.37 ± 0.02	1.38 ± 0.03	4.72 ± 0.04
−0.087			0.374	1.258	4.152
	$Nd_{0.6}Pb_{0.4}MnO_3$ (SC)	[16]	0.374 ± 0.006	1.329 ± 0.003	4.54 ± 0.10
−0.039			0.400	1.311	4.067
	$La_{0.75}Sr_{0.25}MnO_3$ (SC)	[14]	0.40 ± 0.02	1.27 ± 0.06	4.12 ± 0.33
−0.036			0.404	1.314	4.062
	$Pr_{0.70}Pb_{0.30}MnO_3$ (SC)	[17]	0.404 ± 0.001	1.357 ± 0.006	4.73 ± 0.09

[a]PC stands for polycrystalline samples.
[b]SC stands for single-crystal samples.

leading to the expression for the model Hamiltonian as

$$H[\Phi] = \sum_{i=1}^{n} \int \frac{d^d k}{(2\pi)^d} \frac{c_0 \mathbf{k}^2 + r_0}{2} |\phi_i(\mathbf{k})|^2 + \sum_{i=1}^{n} \sum_{j=1}^{n} \iiint \frac{d^d k_1}{(2\pi)^d} \frac{d^d k_2}{(2\pi)^d} \frac{d^d k_3}{(2\pi)^d} \times u(-\mathbf{k}_1 - \mathbf{k}_2) \phi_i(\mathbf{k}_1) \phi_i(\mathbf{k}_2) \times \phi_j(\mathbf{k}_3) \phi_j(-\mathbf{k}_1 - \mathbf{k}_2 - \mathbf{k}_3), \quad (4)$$

with the nonlocal coupling function $u(-\mathbf{k}_1 - \mathbf{k}_2)$ given by Eq. (2).

Following Wilson's scheme, we eliminate the "fast" modes in the momentum shell $\Lambda/b \leqslant q \leqslant \Lambda$, where $b > 1$ and Λ is an ultraviolet cutoff to the momentum integrations. This mode elimination process modifies the parameters of the original Hamiltonian and yields an effective Hamiltonian in terms of the "slow" degrees of freedom in the reduced range $0 \leqslant q \leqslant \Lambda/b$. A subsequent rescaling procedure restores the momentum to the full range $0 \leqslant q \leqslant \Lambda$.

In carrying out this shell elimination procedure, we write the two-point correlation function of the order parameter as [5,6]

$$\langle \phi_i(\mathbf{q}) \phi_j(\mathbf{q}') \rangle_0 = G_0(\mathbf{q}) \delta_{ij} (2\pi)^d \delta^d(\mathbf{q} + \mathbf{q}'), \quad (5)$$

where

$$G_0(\mathbf{q}) = \frac{1}{c_0 \mathbf{q}^2 + r_0} \quad (6)$$

is the (bare) propagator in the momentum shell $\Lambda/b \leqslant q \leqslant \Lambda$.

Elimination of these short-wavelength fluctuations generates the Feynman diagrams shown in Fig. 1. The corresponding self-energy integrals, obtained from their amputated parts (excluding the external legs), are given by

$$\Sigma_a(\mathbf{0}) = 2n \int \frac{d^d q}{(2\pi)^d} u(\mathbf{0}) G_0(\mathbf{q}) \quad (7)$$

and

$$\Sigma_b(\mathbf{k}) = 4 \int \frac{d^d q}{(2\pi)^d} u(-\mathbf{k} - \mathbf{q}) G_0(\mathbf{q}), \quad (8)$$

where the prefactors are combinatorial factors, and the integrals are restricted to the momentum shell $\Lambda/b \leqslant q \leqslant \Lambda$. These self-energy integrals yield the relevant corrections Δr and Δc to the bare parameters r_0 and c_0, given by the expansion

$$\Sigma_a(\mathbf{0}) + \Sigma_b(\mathbf{k}) = \tfrac{1}{2} \Delta r + \tfrac{1}{2} \Delta c\, k^2 + \cdots \quad (9)$$

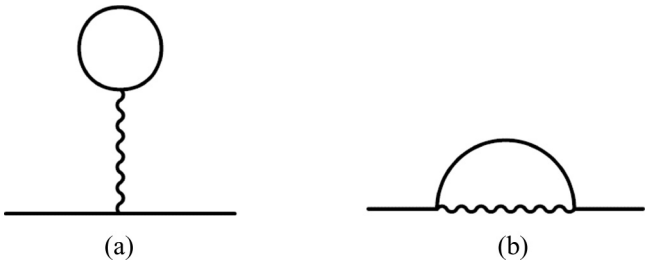

FIG. 1. Feynman diagrams representing the self-energy corrections to r_0 and c_0. The wiggly lines represent $u(\mathbf{0})$ in (a) and $u(-\mathbf{k}-\mathbf{q})$ in (b); the internal solid lines represent correlation $G_0(\mathbf{q})$ between the fast modes.

in the limit $q \gg k$. Employing the expansion

$$u(-\mathbf{k}-\mathbf{q}) = \frac{\lambda_0}{[(\mathbf{k}+\mathbf{q})^2+m^2]^\sigma} = \frac{\lambda_0}{q^{2\sigma}}\left[1 - 2\sigma\frac{\mathbf{k}\cdot\mathbf{q}}{q^2} - \sigma\frac{k^2+m^2}{q^2} + 2\sigma(\sigma+1)\frac{(\mathbf{k}\cdot\mathbf{q})^2}{q^4} + \cdots\right] \tag{10}$$

in the same limit, we obtain from Eqs. (7), (8), and (9)

$$\Delta r = \frac{4n\lambda_0}{m^{2\sigma}}\frac{S_d}{(2\pi)^d}\left[\frac{(b^{2-d}-1)\Lambda^{d-2}}{c_0(2-d)} - \frac{r_0}{c_0^2}\frac{(b^{4-d}-1)\Lambda^{d-4}}{(4-d)}\right] + 8\lambda_0\frac{S_d}{(2\pi)^d}\left[\frac{(b^{2\sigma+2-d}-1)\Lambda^{d-2\sigma-2}}{c_0(2\sigma+2-d)} - \left(\frac{r_0}{c_0^2}+\frac{\sigma m^2}{c_0}\right)\frac{(b^{2\sigma+4-d}-1)\Lambda^{d-2\sigma-4}}{(2\sigma+4-d)}\right] \tag{11}$$

and

$$\Delta c = \frac{8\lambda_0}{c_0}\frac{S_d}{(2\pi)^d}\frac{\sigma(2\sigma+2-d)}{d}\frac{(b^{2\sigma+4-d}-1)\Lambda^{d-4-2\sigma}}{(2\sigma+4-d)}. \tag{12}$$

It may be noted that the n-dependent correction to the bare parameter r_0 comes only from Σ_a given by the first Feynman diagram [Fig. 1(a)].

We also obtain the relevant corrections to the four-point bare interaction vertex $u(-\mathbf{k}_1-\mathbf{k}_2)$. The corresponding one-loop Feynman diagrams are shown in Fig. 2, and their amputated parts (excluding the four external legs) are represented by the integrals

$$\Pi_a(\mathbf{k}_1,\mathbf{k}_2) = -4n\,u^2(-\mathbf{k}_1-\mathbf{k}_2)\int\frac{d^dq}{(2\pi)^d}\,G_0(\mathbf{q}) \times G_0(-\mathbf{k}_1-\mathbf{k}_2-\mathbf{q}), \tag{13}$$

$$\Pi_b(\mathbf{k}_1,\mathbf{k}_2,\mathbf{k}_3) = -16u(-\mathbf{k}_1-\mathbf{k}_2)\int\frac{d^dq}{(2\pi)^d}\,u(\mathbf{q}-\mathbf{k}_3) \times G_0(\mathbf{q})\,G_0(-\mathbf{k}_1-\mathbf{k}_2-\mathbf{q}), \tag{14}$$

and

$$\Pi_c(\mathbf{k}_1,\mathbf{k}_2,\mathbf{k}_3) = -16\int\frac{d^dq}{(2\pi)^d}\,u(-\mathbf{k}_1-\mathbf{q})\,u(\mathbf{q}-\mathbf{k}_2) \times G_0(\mathbf{q})\,G_0(-\mathbf{k}_1-\mathbf{k}_3-\mathbf{q}), \tag{15}$$

where $\mathbf{k}_1$, $\mathbf{k}_2$, $\mathbf{k}_3$, and $\mathbf{k}_4 = -\mathbf{k}_1-\mathbf{k}_2-\mathbf{k}_3$ are the external momenta carried by the four external legs in Fig. 2.

From Eqs. (13), (14), and (15), we see that Π_a and Π_b share the form of the bare vertex $u(-\mathbf{k}_1-\mathbf{k}_2)$ in the original Hamiltonian given by Eq. (4). Consequently, they contribute as a correction $\Delta\lambda$ to the bare parameter λ_0. On the other hand, Π_c is irrelevant as it does not share the form of the bare vertex $u(-\mathbf{k}_1-\mathbf{k}_2)$. This situation is quite unlike the SR case, in which all three diagrams are found to be relevant. It is because of this that the resulting expressions for the LR interaction cannot directly lead to the SR results by substituting $\sigma = 0$.

To eliminate the short-wavelength fluctuations belonging to the high momentum shell $\Lambda/b \leqslant q \leqslant \Lambda$, we expand the integrands in the limit of vanishing external momenta, $k_i \ll q$. The relevant corrections to λ_0, coming from the integrals Π_a and Π_b, yield the correction $\Delta\lambda$ as

$$\Delta\lambda = \frac{-4n\lambda_0^2}{m^{2\sigma}}\frac{S_d}{(2\pi)^d}\left[\frac{(b^{4-d}-1)\Lambda^{d-4}}{c_0^2(4-d)} - \frac{2r_0}{c_0^3}\frac{(b^{6-d}-1)\Lambda^{d-6}}{(6-d)}\right] - 16\lambda_0^2\frac{S_d}{(2\pi)^d}\left[\frac{(b^{2\sigma+4-d}-1)\Lambda^{d-2\sigma-4}}{c_0^2(2\sigma+4-d)} - \left(\frac{\sigma m^2}{c_0^2}+2\frac{r_0}{c_0^3}\right)\frac{(b^{2\sigma+6-d}-1)\Lambda^{d-2\sigma-6}}{(2\sigma+6-d)}\right]. \tag{16}$$

Assuming self-similarity and powerlike falloff of the correlation function at the critical point [5,6] and incorporating the one-loop corrections, given by Eqs. (11), (12), and (16), we obtain the recursion relations for the parameters r, c, and λ as

$$r = b^{2-\eta}(r_0+\Delta r), \quad c = b^{-\eta}(c_0+\Delta c), \quad \lambda = b^{4-d-2\eta+2\sigma}(\lambda_0+\Delta\lambda). \tag{17}$$

Taking $b = e^{\delta l}$, we construct the RG flow equations in the limit $\delta l \to 0$ from Eq. (17) for the scale-dependent parameters $r(l)$, $c(l)$, and $\lambda(l)$, and we arrive at

$$\frac{dr}{dl} = (2-\eta)r + \frac{4n\lambda S_d}{m^{2\sigma}(2\pi)^d}\left(\frac{\Lambda^{d-2}}{c} - \frac{r}{c^2}\Lambda^{d-4}\right) + \frac{8\lambda S_d}{(2\pi)^d}\left[\frac{\Lambda^{d-2-2\sigma}}{c} - \left(\frac{r}{c^2}+\frac{\sigma m^2}{c}\right)\Lambda^{d-4-2\sigma}\right], \tag{18}$$

$$\frac{dc}{dl} = -\eta c + \frac{8\sigma(2\sigma+2-d)\lambda S_d}{d(2\pi)^d}\frac{\Lambda^{d-4-2\sigma}}{c}, \tag{19}$$

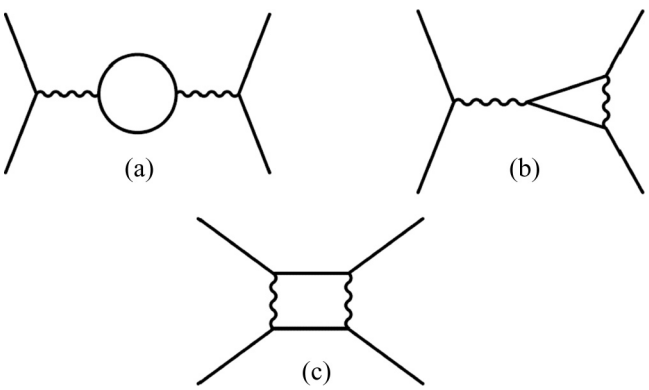

FIG. 2. Feynman diagrams representing corrections to the vertex $u(-\mathbf{k}_1-\mathbf{k}_2)$ at one-loop order.

and

$$\frac{d\lambda}{dl} = (4-d-2\eta+2\sigma)\lambda - \frac{4n\lambda^2 S_d}{m^{2\sigma}(2\pi)^d}\left(\frac{\Lambda^{d-4}}{c^2} - \frac{2r}{c^3}\Lambda^{d-6}\right) - \frac{16\lambda^2 S_d}{(2\pi)^d}\left[\frac{\Lambda^{d-4-2\sigma}}{c^2} - \left(\frac{2r}{c^3} + \frac{\sigma m^2}{c^2}\right)\Lambda^{d-6-2\sigma}\right]. \quad (20)$$

Solving the above flow equations for the nontrivial fixed point $(r^*,\lambda^*,c^*=c)$, we obtain

$$\frac{r^*}{c} = -\frac{(4-d-2\eta+2\sigma)\left\{\frac{4n}{w^\sigma} + 8(1-\frac{\sigma w}{c})\right\}\Lambda^2}{(2-\eta)\left\{\frac{4n}{w^\sigma} + 16(1-\sigma w)\right\} - (4-d-2\eta+2\sigma)\left(\frac{4n}{w^\sigma}+8\right)} \quad (21)$$

and

$$\frac{\lambda^*}{c^2} = \frac{(4-d-2\eta+2\sigma)\Lambda^{4-d+2\sigma}}{\frac{S_d}{(2\pi)^d}\left\{\frac{4n}{w^\sigma} + 16(1-\sigma w)\right\}}, \quad (22)$$

where $w = m^2/\Lambda^2$ is a redefined dimensionless screening parameter. A linear stability analysis around the nontrivial fixed point yields the eigenvalues y_1 and y_2 as

$$y_1 = 2-\eta-(4-d-2\eta+2\sigma)\frac{\left(\frac{4n}{w^\sigma}+8\right)}{\left[\frac{4n}{w^\sigma} + 16(1-\sigma w)\right]} \quad (23)$$

and

$$y_2 = d-4+2\eta-2\sigma. \quad (24)$$

Here y_1 and y_2 correspond, respectively, to unstable and stable eigendirections in the RG flow. We identify the upper critical dimension d_c from the marginal stability of the stable eigenvalue y_2, giving

$$d_c = 4+2\sigma. \quad (25)$$

The stability analysis coupled with the conditions $y_1 \geq 0$ and $y_2 \leq 0$ impose restrictions on the allowed values of σ. For $d=n=3$, we find that the value of σ is restricted in the range $-0.50 \leq \sigma \leq 0.51$ and, for $d=2$ and $n=3$, it is restricted in the range $-1.00 \leq \sigma \leq 0.16$ for small values of the screening parameter w. These stability ranges are somewhat insensitive to the values of n and w. We shall see that the critical exponents for many experimental perovskite manganite samples are obtained in the negative range of σ for $d=3$. In the following section, we calculate the critical exponents in an ϵ expansion scheme with the identification

$$\epsilon = d_c - d. \quad (26)$$

III. CALCULATION OF CRITICAL EXPONENTS

We obtain the critical exponent ν, occurring in the correlation length $\xi \sim |T-T_c|^{-\nu}$, from the unstable eigenvalue y_1 [given by Eq. (23)] using the relation $\nu = 1/y_1$, so that

$$\nu = \frac{1}{2} + \frac{\epsilon\left(\frac{n}{w^\sigma}+2\right)}{2\left[\frac{n}{w^\sigma}+4(1-\sigma w)\right]}\left\{\frac{1}{2} + \frac{2\sigma}{(\sigma+2)\left[\frac{n}{w^\sigma}+4(1-\sigma w)\right]-4\sigma}\right\} - \frac{\sigma\epsilon}{2(\sigma+2)\left[\frac{n}{w^\sigma}+4(1-\sigma w)\right]-8\sigma} + O(\epsilon^2), \quad (27)$$

with the expansion parameter $\epsilon = 4-d+2\sigma$. The Fisher exponent η is obtained from Eq. (19) by setting $dc/dl = 0$, and we find

$$\eta = -\frac{2\sigma\epsilon}{(\sigma+2)\left[\frac{n}{w^\sigma}+4(1-\sigma w)\right]-4\sigma} + O(\epsilon^2). \quad (28)$$

It is interesting to note that we obtain a nonzero value for the exponent η in the first order of ϵ. This is in contrast with the calculation of Fisher, Ma, and Nickel [9], where η does not get any correction even up to $O(\epsilon'^3)$, where $\epsilon' = 2\sigma' - d$.

Using Eqs. (27) and (28) and the well-known Fisher, Widom, Rushbrooke, and Josephson scaling laws [5,6,8,42], we calculate the other critical exponents, namely the specific-heat exponent α, the spontaneous magnetization exponent β, the susceptibility exponent γ, and the critical isotherm exponent δ, and we obtain

$$\alpha = \frac{\epsilon+4}{2} - (\sigma+2)\left[1 + \frac{\epsilon(\frac{n}{w^\sigma}+2)}{\frac{n}{w^\sigma}+4(1-\sigma w)}\left\{\frac{1}{2} + \frac{2\sigma}{(\sigma+2)\left[\frac{n}{w^\sigma}+4(1-\sigma w)\right]-4\sigma}\right\} - \frac{\sigma\epsilon}{(\sigma+2)\left[\frac{n}{w^\sigma}+4(1-\sigma w)\right]-4\sigma}\right] + O(\epsilon^2), \quad (29)$$

$$\beta = \frac{\sigma+1}{2} - \frac{\epsilon}{4}\left[1 + \frac{2\sigma(\sigma+2)}{(\sigma+2)\left[\frac{n}{w^\sigma}+4(1-\sigma w)\right]-4\sigma} - \frac{\left(\frac{n}{w^\sigma}+2\right)(2\sigma+2)}{\frac{n}{w^\sigma}+4(1-\sigma w)}\left\{\frac{1}{2} + \frac{2\sigma}{(\sigma+2)\left[\frac{n}{w^\sigma}+4(1-\sigma w)\right]-4\sigma}\right\}\right] + O(\epsilon^2), \quad (30)$$

$$\gamma = 1 + \frac{\epsilon\left(\frac{n}{w^\sigma}+2\right)}{\frac{n}{w^\sigma}+4(1-\sigma w)}\left[\frac{1}{2} + \frac{2\sigma}{(\sigma+2)\left[\frac{n}{w^\sigma}+4(1-\sigma w)\right]-4\sigma}\right] + O(\epsilon^2), \quad (31)$$

$$\delta = \frac{\sigma+3}{\sigma+1} + \frac{\epsilon}{\sigma+1}\left[\frac{1}{\sigma+1} + \frac{2\sigma(\sigma+2)}{(\sigma+1)\left[(\sigma+2)\left\{\frac{n}{w^\sigma}+4(1-\sigma w)\right\}-4\sigma\right]}\right] + O(\epsilon^2). \quad (32)$$

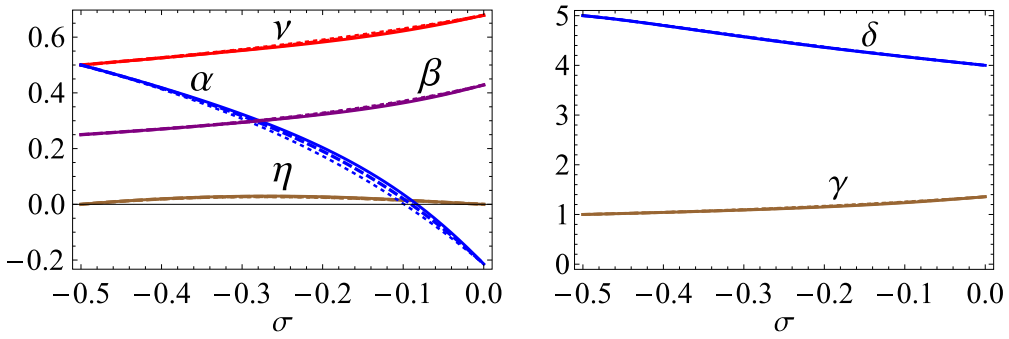

FIG. 3. (Color online) Critical exponents (a) ν, η, α, β, and (b) γ, δ for $n = 3$ and $d = 3$ for three different values of the screening parameter w. The solid, dashed, and dotted curves correspond to $w = 0.0001$, 0.001, and 0.01, respectively. The curves can be distinguished only for the exponent α; they cannot be distinguished for the other exponents due to insufficient resolution.

We see that the analytical forms of the critical exponents, given by Eqs. (27)–(32), depend on the parameters n, d, σ, and w. In these expressions, the terms containing w and n do not vary strongly for different values of w and n. This is demonstrated in the graphical plots in Fig. 3, where the critical exponents show slow variation with respect to w for a range of σ relevant to the experimental samples given in Table II. In addition, we see that although the exponents ν, α, and β undergo slight variation with respect to n (in the vicinity of $\sigma = 0$), the exponents η, γ, and δ show insignificant variation, as displayed in Fig. 4.

From our results, we see for the marginal case of $\epsilon = 0$ in $d = 3$ that the values of the critical exponents match almost exactly with those of tricritical mean-field exponents [24], namely $\alpha = \frac{1}{2}$, $\beta = \frac{1}{4}$, $\gamma = 1$, and $\delta = 5$. It may be noted that this result for the tricritical point is independent of the screening parameter w because it occurs in the $O(\epsilon)$ terms in the ϵ expansions. The analytical results for the critical exponents, following from Eqs. (30), (31), and (32), are compared with the experimental estimates [10–23] in Table II. To compare the experimental estimates with our theoretical results for the critical exponents β, γ, and δ, we first match the value of β. For a particular sample, we obtain from Eq. (30) the experimental β value (up to three significant figures) for a particular value of σ. Using this value of σ, we calculate the values of γ and δ (for the same sample) from Eqs. (31) and (32), respectively. We find that for a range of experimental values of β, the corresponding values of γ and δ are comparable to those of the experimental values for $n = 3$ in three dimensions for $w = 0.001$. The agreement of our results with the experimental values indicates that the nonlocal model Hamiltonian is capable of capturing a wide range of universality classes for a wide variety of perovskite manganite samples.

It may also be noted that if we had not taken the screening explicitly into account in the model, the agreement for the critical exponents would be greatly reduced over the wide range of experimental samples. In particular, for samples away from the tricritical mean-field behavior, we found that the values of γ and δ obtained from a model without screening, as in Ref. [52], would deviate farther from the experimental numbers. This signifies that screening plays a fundamental role in determining the critical exponents in perovskite manganites.

IV. DISCUSSION AND CONCLUSION

Employing Wilson's RG scheme, we investigated the critical behavior of a modified Ginzburg-Landau model [Eq. (1)] incorporating a nonlocal interaction in the quartic (Φ^4) term as suggested by Ma [5]. We modeled the interaction term with a nonlocal character coupled with a screening parameter m and an exponent σ [Eq. (2)]. As a result, we obtained

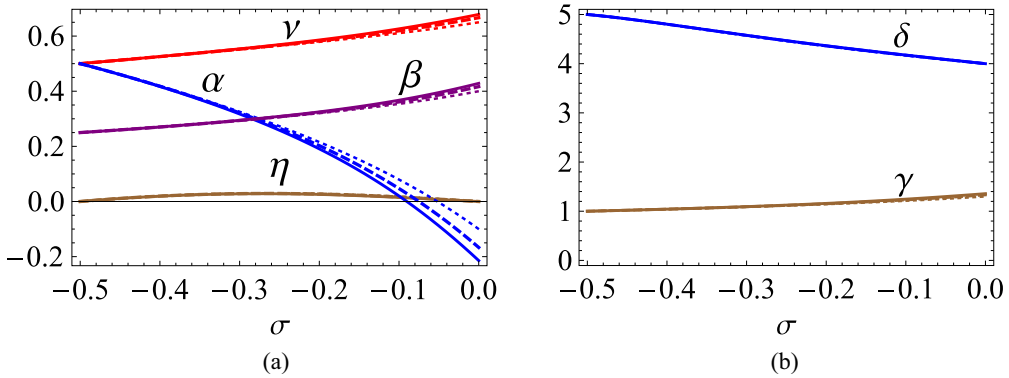

FIG. 4. (Color online) Critical exponents (a) ν, η, α, β and (b) γ, δ for $w = 0.001$, and $d = 3$ for three different values of n. The dotted, dashed, and solid curves correspond to $n = 1$, 2, and 3, respectively. The curves can be distinguished only for the exponents ν, α, and β; they cannot be distinguished for the other exponents due to insufficient resolution.

the renormalization corrections to the bare parameters r_0, λ_0, and c_0 in the model Hamiltonian. The ensuing RG flow equations led to the existence of a nontrivial fixed point, and the marginal stability of the stable eigenvalue gave the upper critical dimension as $d_c = 4 + 2\sigma$. We calculated the critical exponents ν, η, α, β, γ, and δ at $O(\epsilon)$ via an ϵ expansion in the parameter $\epsilon = d_c - d$, and we found that the screening parameter $w = m^2/\Lambda^2$ plays some role in determining the critical exponents. However, the variations of the critical exponents with respect to w are slow, as is evident from the graphical plots of the exponents in Fig. 3. In addition, although the exponents ν, α, and β undergo slight variations with n in the neighborhood of $\sigma = 0$ (as shown in Fig. 4), these variations are insignificant compared to those of the short-range models, namely the 3D Ising and 3D Heisenberg models.

We have compared our results with the experimentally available estimates for the critical exponents β, γ, and δ, and we found that our analytical estimates are in good agreement with those of the experiments for a wide variety of perovskite manganite samples, including those showing tricritical mean-field exponents. We can consider the agreement to be very good when we look at the nature of the approximation involved in our RG calculations in that it is only at $O(\epsilon)$ and the higher-order terms in ϵ are neglected. We have thus shown that the leading order in ϵ captures the correct trend of the critical exponents both near and away from tricriticality, as observed experimentally in a wide range of perovskite manganite samples. We expect more exact agreement with the experimental numbers if we include the higher-order terms in the ϵ expansion. However, that would require a vast amount of calculations, probably up to four- or five-loop orders, so that a meaningful Borel summation of the ϵ expansion could be performed. We deem such a detailed and exact calculation of critical exponents unnecessary at this stage as we are interested in identifying the correct form of the Hamiltonian capable of explaining the wide variety of universality classes of perovskite manganites. Since our RG results, at $O(\epsilon)$, have been able to capture a wide range of critical exponents comparable with experiments, it is fair to guess that the corresponding model Hamiltonian, given by Eqs. (1) and (2), contains a wide diversity of universality classes relevant to perovskite manganite samples.

It is interesting to note from the experiments that a change in doping level x as well as the elements (R and/or A) in the composition in perovskite manganites $R_{1-x}A_x\mathrm{MnO_3}$ lead to different critical exponents. Different choices for R and A have different atomic sizes and therefore produce different internal stresses on the Mn-O-Mn bond [43–45]. This is characterized by the tolerance factor $f = (\langle r_A\rangle + r_\mathrm{O})/[\sqrt{2}(r_\mathrm{Mn} + r_\mathrm{O})]$ that compares the Mn-O separation with the separation of the oxygen atom and the A-site occupant. Thus, a change in either the doping level (x) or the tolerance factor (f) is found to lead to different universality classes. Our analytical calculations with the nonlocal model Hamiltonian are capable of reproducing the experimental results for different values of the nonlocal parameter σ, as shown in Table II. It appears that the model parameter σ has a close connection with the experimental parameters x and f. However, finding this connection seems to pose further challenges because it requires the derivation of the nonlocal model Hamiltonian from a more microscopic Hamiltonian containing finer details that are to be eliminated as irrelevant degrees of freedom to arrive at the (less microscopic) nonlocal model Hamiltonian. This will be similar to the case of justifying the GL model for superconductivity from the microscopic BCS theory [46]. However, since our nonlocal model Hamiltonian captures a wide range of experimental observations, we shall not delve into such a justification of the Hamiltonian from a more microscopic theory. This is in line with the notions and practices in condensed-matter physics, where the detailed microscopic origins of model Hamiltonians are usually deemed unnecessary.

We would also like to note that the experiments performed to study PM-FM phase transitions in perovskite manganites were based on four different techniques, namely neutron scattering [10], dc magnetization [11], ac susceptibility [15], and specific-heat [13] measurements, followed by scaling analysis with the Arrot plot, the modified Arrot plot [12,13], the Kouvel-Fisher formalism, and the study of critical isotherms [15,19]. However, measurably different results were obtained from such experiments on the sample $\mathrm{La_{0.7}Sr_{0.3}MnO_3}$ [10,11,47,48]. Notably, four different sets of values for the critical exponents in the experiments were $\beta = 0.295 \pm 0.002$ in Ref. [10]; $\beta = 0.37 \pm 0.04$, $\gamma = 1.22 \pm 0.03$, and $\delta = 4.25 \pm 0.2$ in Ref. [11]; $\beta = 0.45 \pm 0.01$, $\gamma = 1.2$, and $\delta = 3.901$ in Ref. [47]; and $\beta = 0.45 \pm 0.02$ and $\gamma = 1.08 \pm 0.04$ in Ref. [48], showing significant variations in the critical exponents for the same experimental sample. Similar disagreements between experimental results were also observed in the sample $\mathrm{La_{0.8}Ca_{0.2}MnO_3}$ [12,20] for which $\beta = 0.36$, $\gamma = 1.45$, and $\delta = 5.03$ in Ref. [12] and $\beta = 0.328$, $\gamma = 1.193$, and $\delta = 4.826$ in Ref. [20]. Such disagreement was also observed for the case of $\mathrm{La_{0.7}Ca_{0.3}MnO_3}$ [47,49] for which $\beta = 0.14$, $\gamma = 1.2$, and $\delta = 1.22 \pm 0.02$ in Ref. [49] and $\beta = 0.36$ and $\gamma = 1.2$ in Ref. [47]. This indicates that additional experimental studies with high-purity samples accompanied by more refined data analysis are required to rectify such experimental discrepancies.

In addition, we observe that the results $\beta = 0.5 \pm 0.02$, $\gamma = 1.08 \pm 0.03$, and $\delta = 3.13 \pm 0.20$ for $\mathrm{La_{0.8}Sr_{0.2}MnO_3}$ [50] are close to the mean-field results ($\beta = \frac{1}{2}$, $\gamma = 1$, and $\delta = 3$) [5]. We note that the mean-field results cannot be reproduced by the present nonlocal theory. Since the present theory is an expansion about the tricritical point, it captures the critical behavior near and around the tricritical point. Moreover, the results of Ref. [49] cannot be explained by the present theory as they deviate strongly from the Widom scaling law, where the δ value is too low ($\delta = 1.22$), with $\beta = 0.14$ and $\gamma = 0.81$. Additionally, Ref. [51] presents the results for the Griffith phase in $\mathrm{La_{1-x}Ca_xMnO_3}$ for $x = 0.21$ with unusual exponents $\beta = 0.09 \pm 0.01$, $\gamma = 1.71 \pm 0.1$, and $\delta = 20 \pm 1$. In contrast, it may be mentioned that for a slightly different value $x = 0.2$, this compound exhibits the usual behavior of perovskite manganites as observed in Refs. [12,20].

Finally, we would like to conclude by noting that the wide diversity in the critical behavior observed in perovskite manganites poses a challenging task for its description by means of a theoretical framework. As we have shown, within the context of a phenomenological model Hamiltonian with a nonlocal screened coupling in the quartic interaction term, it is possible to capture such diversity

in the critical behavior for a wide range of experimental samples. We hope that our results would inspire further experimental work for further verification of the critical exponents.

ACKNOWLEDGMENTS

R.S. is thankful to the Ministry of Human Resource Development (MHRD), Government of India, for financial support through a scholarship.

[1] K. G. Wilson and M. E. Fisher, Phys. Rev. Lett. **28**, 240 (1972).
[2] K. G. Wilson, Phys. Rev. Lett. **28**, 548 (1972).
[3] S.-k. Ma, Rev. Mod. Phys. **45**, 589 (1973).
[4] K. G. Wilson and J. Kogut, Phys. Rep. **12**, 75 (1974).
[5] S.-k. Ma, *Modern Theory of Critical Phenomena* (Benjamin, Reading, MA, 1976).
[6] N. Goldenfeld, *Lectures on Phase Transitions and the Renormalization Group* (Addison-Wesley, Reading, MA, 1992).
[7] J. Zinn-Justin, *Quantum Field Theory and Critical Phenomena* (Oxford University Press, Oxford, 2002).
[8] M. Kardar, *Statistical Physics of Fields* (Cambridge University Press, Cambridge, 2007).
[9] M. E. Fisher, S.-k. Ma, and B. G. Nickel, Phys. Rev. Lett. **29**, 917 (1972).
[10] M. C. Martin, G. Shirane, Y. Endoh, K. Hirota, Y. Moritomo, and Y. Tokura, Phys. Rev. B **53**, 14285 (1996).
[11] K. Ghosh, C. J. Lobb, R. L. Greene, S. G. Karabashev, D. A. Shulyatev, A. A. Arsenov, and Y. Mukovskii, Phys. Rev. Lett. **81**, 4740 (1998).
[12] C. S. Hong, W. S. Kim, and N. H. Hur, Phys. Rev. B **63**, 092504 (2001).
[13] D. Kim, B. Revaz, B. L. Zink, F. Hellman, J. J. Rhyne, and J. F. Mitchell, Phys. Rev. Lett. **89**, 227202 (2002).
[14] D. Kim, B. L. Zink, F. Hellman, and J. M. D. Coey, Phys. Rev. B **65**, 214424 (2002).
[15] S. Nair, A. Banerjee, A. V. Narlikar, D. Prabhakaran, and A. T. Boothroyd, Phys. Rev. B **68**, 132404 (2003).
[16] M. Sahana, U. K. Rössler, N. Ghosh, S. Elizabeth, H. L. Bhat, K. Dörr, D. Eckert, M. Wolf, and K.-H. Müller, Phys. Rev. B **68**, 144408 (2003).
[17] B. Padmanabhan, H. L. Bhat, S. Elizabeth, S. Rößler, U. K. Rößler, K. Dörr, and K. H. Müller, Phys. Rev. B **75**, 024419 (2007).
[18] R. Venkatesh, M. Pattabiraman, K. Sethupathi, G. Rangarajan, S. Angappane, and J.-G. Park, J. Appl. Phys. **103**, 07B319 (2008).
[19] J. Fan, L. Ling, B. Hong, L. Zhang, L. Pi, and Y. Zhang, Phys. Rev. B **81**, 144426 (2010).
[20] M. Khlifi, A. Tozri, M. Bejar, E. Dhahri, and E. K. Hlil, J. Magn. Magn. Mater. **324**, 2142 (2012).
[21] M. Nasri, M. Triki, E. Dhahri, and E. K. Hlil, J. Alloys Compd. **546**, 84 (2013).
[22] M. Smari, I. Walha, A. Omri, J. J. Rousseau, E. Dhahri, and E. K. Hlil, Ceram. Int. **40**, 8945 (2014).
[23] Za. Mohamed, E. Tka, J. Dhahri, and E. K. Hlil, J. Alloys. Compd. **619**, 520 (2015).
[24] K. Huang, *Statistical Mechanics*, 2nd ed. (Wiley, New York, 1987).
[25] M. Suzuki, Y. Yamazaki, and G. Igarashi, Phys. Lett. A **42**, 313 (1972).
[26] J. Sak, Phys. Rev. B **8**, 281 (1973).
[27] A. Aharony, Phys. Rev. B **9**, 2416 (1974).
[28] A. Theumann, J. Phys. A **14**, 2759 (1981).
[29] J. K. Bhattacharjee, J. L. Cardy, and D. J. Scalapino, Phys. Rev. B **25**, 1681 (1982).
[30] M. A. Gusmão and W. K. Theumann, Phys. Rev. B **28**, 6545 (1983).
[31] J. Honkonen, J. Phys. A **23**, 825 (1990).
[32] S. V. Belim, JETP Lett. **77**, 112 (2003).
[33] E. Luijten, H. W. J. Blöte, and K. Binder, Phys. Rev. E **54**, 4626 (1996).
[34] E. Luijten and H. W. J. Blöte, Phys. Rev. Lett. **76**, 1557 (1996).
[35] E. Luijten and H. W. J. Blöte, Phys. Rev. B **56**, 8945 (1997).
[36] E. Luijten and H. W. J. Blöte, Phys. Rev. Lett. **89**, 025703 (2002).
[37] A. Tröster, Phys. Rev. E **79**, 036707 (2009).
[38] A. Tröster, Phys. Rev. B **81**, 125135 (2010).
[39] M. Picco, arXiv:1207.1018 (2012).
[40] T. Blanchard, M. Picco, and M. A. Rajabpour, Europhys. Lett. **101**, 56003 (2013).
[41] A. Tröster, Phys. Rev. Lett. **100**, 140602 (2008).
[42] D. J. Amit and V. Martin-Mayor, *Field Theory, the Renormalization Group, and Critical Phenomena*, 3rd ed. (World Scientific, Singapore, 2005).
[43] A. J. Millis, Nature (London) **392**, 147 (1998).
[44] N. A. Babushkina, L. M. Belova, O. Yu. Gorbenko, A. R. Kaul, A. A. Bosak, V. I. Ozhogin, and K. I. Kugel, Nature (London) **391**, 159 (1998).
[45] M. B. Salamon and M. Jaime, Rev. Mod. Phys. **73**, 583 (2001).
[46] L. P. Gor'kov, Sov. Phys. JETP **9**, 1364 (1959).
[47] S. Taran, B. K. Chaudhuri, S. Chatterjee, H. D. Yang, S. Neeleshwar, and Y. Y. Chen, J. Appl. Phys. **98**, 103903 (2005).
[48] M. Ziese, J. Phys.: Condens. Matter **13**, 2919 (2001).
[49] H. S. Shin, J. E. Lee, Y. S. Nam, H. L. Ju, and C. W. Park, Solid State Commun. **118**, 377 (2001).
[50] Ch. V. Mohan, M. Seeger, H. Kronmüller, P. Murugaraj, and J. Maier, J. Magn. Magn. Mater. **183**, 348 (1998).
[51] W. Jiang, X. Z. Zhou, G. Williams, Y. Mukovskii, and K. Glazyrin, Phys. Rev. Lett. **99**, 177203 (2007).
[52] R. Singh, K. Dutta, and M. K. Nandy, Europhys. Lett. **110**, 16003 (2015).